

# Crystal Structures of MEK1 Binary and Ternary Complexes with Nucleotides and Inhibitors

Thierry O. Fischmann,<sup>\*,‡</sup> Catherine K. Smith,<sup>\*,‡,§</sup> Todd W. Mayhood, Joseph E. Myers, Jr.,<sup>||</sup> Paul Reichert, Anthony Mannarino, Donna Carr, Hugh Zhu, Jesse Wong, Rong-Sheng Yang, Hung V. Le, and Vincent S. Madison

Schering-Plough Research Institute, 2015 Galloping Hill Road, Kenilworth, New Jersey 07033

Received October 8, 2008; Revised Manuscript Received January 16, 2009

**ABSTRACT:** MEK1 is a member of the MAPK signal transduction pathway that responds to growth factors and cytokines. We have determined that the kinase domain spans residues 35–382 by proteolytic cleavage. The complete kinase domain has been crystallized and its X-ray crystal structure as a complex with magnesium and ATP- $\gamma$ S determined at 2.1 Å. Unlike crystals of a truncated kinase domain previously published, the crystals of the intact domain can be grown either as a binary complex with a nucleotide or as a ternary complex with a nucleotide and one of a multitude of allosteric inhibitors. Further, the crystals allow for the determination of costructures with ATP competitive inhibitors. We describe the structures of nonphosphorylated MEK1 (npMEK1) binary complexes with ADP and K252a, an ATP-competitive inhibitor (see Table 1), at 1.9 and 2.7 Å resolution, respectively. Ternary complexes have also been solved between npMEK1, a nucleotide, and an allosteric non-ATP competitive inhibitor: ATP- $\gamma$ S with compound **1** and ADP with either U0126 or the MEK1 clinical candidate PD325089 at 1.8, 2.0, and 2.5 Å, respectively. Compound **1** is structurally similar to PD325901. These structures illustrate fundamental differences among various mechanisms of inhibition at the molecular level. Residues 44–51 have previously been shown to play a negative regulatory role in MEK1 activity. The crystal structure of the integral kinase domain provides a structural rationale for the role of these residues. They form helix A and repress enzymatic activity by stabilizing an inactive conformation in which helix C is displaced from its active state position. Finally, the structure provides for the first time a molecular rationale that explains how mutations in MEK may lead to the cardio-facio-cutaneous syndrome.

MEK1 functions as one of several important mediators of signal transduction that controls cell proliferation (1–46), cell differentiation (3, 7, 8), and early embryonic development. It is a member of the mitogen-activated protein kinase (MAPK)<sup>1</sup> cascade, a highly conserved eukaryotic signaling pathway, that links cellular responses to extracellular stimuli such as growth factors and cytokines (9, 10). The pathway is organized as evolutionarily conserved modules composed of three sequentially activating kinases: an upstream MAPK kinase kinase (MAPKKK, Raf) which phosphorylates and activates the MAPK kinase (MAPKK), also named MAPK ERK kinase (MEK), which in turn phosphorylates and activates the extracellular signal-regulated MAPK kinase (ERK) (10). The MEK/ERK signaling module is the predominant MAPK pathway mediating responses to both proliferative and differentiative signals (11, 12).

MEK1/2 are dual specificity kinases that activate ERK1/2 via phosphorylation of Thr and Tyr residues in the regulatory activating lip or T-loop (TEY) of ERK1/2 (13). Unlike many

other kinases, MEK1/2 apparently require both the correct T-loop residues and the native ERK1/2 tertiary fold for recognition and phosphorylation. MEK1/2 do not phospho-

<sup>1</sup> Abbreviations: Abl, Abelson tyrosine kinase; ATP, adenosine 5'-triphosphate; ADP, adenosine 5'-diphosphate; AMP-PNP, adenosine 5'-( $\beta,\gamma$ -imido)triphosphate; AMP-PCP,  $\beta,\gamma$ -methyleneadenosine 5'-triphosphate; ATP- $\gamma$ S, adenosine 5'-[ $\gamma$ -thio]triphosphate; AMP, adenosine monophosphate; cAK, cyclic adenosine monophosphate-dependent protein kinase; CD, circular dichroism; CDK, cyclin-dependent kinase; CFC, cardio-facio-cutaneous; CK, casein kinase; DMSO, dimethyl sulfoxide; DSC, differential scanning calorimetry; DTT, dithiothreitol; ERK, extracellular regulatory kinase; ESI-MS, electrospray ionization mass spectrometry; FAK, focal adhesion kinase; FGFR TK, fibroblast growth factor receptor tyrosine kinase; GSK-3 $\beta$ , glycogen synthase kinase-3 $\beta$ ; HCK, hemopoietic cell kinase; HEPES, *N*-(2-hydroxyethyl)piperazine-*N'*-2-ethanesulfonic acid; HM, hydrophobic motif; ITC, isothermal titration calorimetry; JNK, c-Jun N-terminal kinase; LCK, lymphocyte-specific protein tyrosine kinase; LC-MS, liquid chromatography–mass spectrometry; MAP, mitogen-activated kinase; MAPK, mitogen-activated protein kinase; MAPKK, mitogen-activated protein kinase kinase; MEK, MAPK ERK kinase; NES, nuclear export signal; NMR, nuclear magnetic resonance spectroscopy; npMEK1, nonphosphorylated MEK1; PAK, p21-activated kinase; PDGF, platelet-derived growth factor; PKA, protein kinase A; pMEK1, phosphorylated MEK1; RMS, root mean square; SDS, sodium dodecyl sulfate; TCEP, tris(2-carboxyethyl)phosphine hydrochloride; TGF $\beta$ RTK, transforming growth factor- $\beta$  receptor tyrosine kinase; VEGFR, vascular endothelial growth factor receptor; VEGFR TK, vascular endothelial growth factor receptor tyrosine kinase; Ala (A), alanine; Asp (D), aspartic acid; Asn (N), asparagine; Glu (E), glutamic acid; Leu (L), leucine; Lys (K), lysine; Met (M), methionine; Phe (F), phenylalanine; pThr, phosphorylated threonine; Pro (P), proline; Ser (S), serine; Thr (T), threonine; Tyr (Y), tyrosine; Val (V), valine.

\* Corresponding authors. T.O.F.: telephone, (908) 740-3603; fax, (908) 740-2616; e-mail, thierry.fischmann@spcorp.com. C.K.S.: telephone, (732) 594-4934; fax, (732) 594-1144; e-mail, catherine\_smith3@merck.com.

<sup>‡</sup> Both authors have contributed significantly to this publication.

<sup>§</sup> Current address: Merck Research Laboratories, 126 East Lincoln Ave., P.O. Box 2000 RY80M-190, Rahway, NJ 07065.

<sup>||</sup> Current address: Bristol-Myer Squibbs, Route 206 and Province Line Road, Princeton, NJ 08540.



FIGURE 1: Organization of the MEK1 protein. The arrows represent the positions where proteolytic cleavage occurs.

rylate ERK1/2 peptides nor do they phosphorylate denatured ERK1/2 (14). The interaction between MEK1/2 and ERK1/2 is unusually specific: MEK1/2 are the only known activators of ERK1/2, and ERK1/2 are the only known substrates of MEK1/2 (9, 15).

An important feature of protein kinases is that they exist in at least two activity states (high and low) that are regulated by phosphorylation of the protein. The high and low activity states can adopt different conformations which can interact with ligands and inhibitors differently. Hence, a full understanding of the inhibition mechanism requires evaluating the binding of inhibitors to both the active and inactive states. MEK1/2 are regulated and activated by Raf phosphorylation of two serine residues in the T-loop, Ser 218 and Ser 222 (SMANS) (16, 17). Phosphorylation of both serine residues is required for activation (18). The dephosphorylated form of MEK1/2 has extremely low activity, which is increased 5000-fold after maximal phosphorylation with c-Raf in a coupled assay (17). Substitution of the T-loop serine residues with negatively charged amino acids, such as aspartate or glutamate, partially mimics phosphorylation and results in a constitutively active kinase (3, 5, 19, 20). For example, the specific activity of the S218D/S222D MEK1 is 300-fold greater than the basal activity of the wild-type enzyme (21).

MEK1/2 kinases contain a variety of features and domains in addition to the core kinase region. These include an ERK docking region, a negative regulatory region, a Pro-rich insert in the kinase domain, and a nuclear export sequence inserted in the core kinase domain. Figure 1 illustrates these features. The function and location of these MEK1/2 regions have been defined through many elegant mutational and enzymatic studies. The ERK2 docking site is located near the N-terminus within the first 31 residues of MEK1 (5, 21, 22). The nuclear export signal (NES) is located between residues 32–44 and appears to be required for cytoplasmic localization (and nuclear exclusion) of MEK (23, 24). The NES is followed by the overlapping regulatory region, amino acids 32–51, the role of which will be discussed further below. Based on sequence homology, residues 53–369 are part of the core kinase domain. Finally, the function of the C-terminal residues is still unclear. Kinase domains truncated at the C-terminus to residue 343, 358, 363, 367, or 373 show wild-type basal ATPase activity but cannot be activated by v-Mos (21). This result suggests that the C-terminal region contains a recognition motif for the activating kinase of MEK1. It has also been proposed that the C-terminal region contains a cellular translocation signal (25).

The role of residues 32–51 has been elucidated in a series of mutagenesis experiments. MEK1 deletions within this region result in constitutive phosphorylation activity toward ERK2 (5, 21). In combination with the mutations S218D, M219D, N221D, and S222D, the MEK1 deletion mutant  $\Delta 44$ –51 (deletion of residue 44–51) exhibits a basal activity that is increased 2300-fold versus wild type. Replacement of the negative regulatory region amino acids ( $\Delta 32$ –51,  $\Delta 44$ –51, or  $\Delta 47$ –49) with polyAla maintains the enzyme in an inactive state while deletion of those same residues

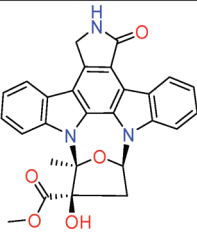
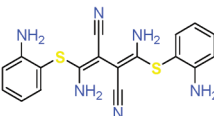
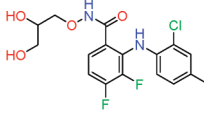
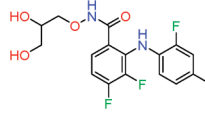
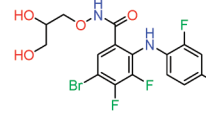
produces a constitutively active protein (21). Substitution of amino acids 47–49 with Pro yields a constitutively active protein. Apparently, this region is important for maintaining the enzyme in an inactive state, and the identity of the side chains is less important than the integrity of the secondary structure itself. Secondary structure predictions and mutagenesis experiments suggest that residues 32–51 form a helix. There have been no data available to understand these results at the structural level prior to the study presented here.

Sequence alignment of MEK1 with other kinases shows that residues 55–369 following the negative regulatory helix constitute the consensus core kinase domain (see Results). The crystal structure of the ternary complex of MEK1 (62–393), ATP, and an allosteric inhibitor, PD318088, has been solved (26). Analysis of the MEK1 ternary complex crystal structure indicates that PD318088 and PD184352-like inhibitors “bind and stabilize a naturally occurring inactive conformation of the protein”. Because the structures of apo, nucleotide only, or phosphorylated MEK1 (pMEK1) have not been determined, it is difficult to differentiate between native and inhibitor-induced alterations to the classical kinase fold. Nevertheless, the reported X-ray structures for the nonphosphorylated state in complex with PD184352-like inhibitors (PD313088, PD334581) suggest that these inhibitors can bind to a low activity form of MEK1 with significant conformational changes at the beginning of the activation loop and a shift in the location of helix C (26) (see Table 1).

There are many non-ATP competitive MEK1 inhibitors including U0126 and PD325901 (9, 27–31, 33). Apparently, the allosteric site accommodates a variety of chemotypes and molecular sizes. Thermodynamic studies show dramatic differences in energy contributions between U0126 and PD325901 bound MEK1·nucleotide complexes (34). PD325901 presents a synergistic stabilizing effect in the formation of the ternary complex while U0126 shows a straightforward additive stabilization: MEK1 binds U0126 and nucleotide in an additive stabilizing mode where the  $\Delta T_m$  of the complex equals the sum of the  $\Delta T_m$ 's of each binary complex. Thermodynamic studies suggest that the inhibitors may present key differences in interactions with the nucleotide. But so far no crystal structure of the MEK1·U0126·nucleotide ternary complex has been available to give a firm structural basis for the different modes of inhibition.

In this study, we establish the domain boundaries of the MEK1 kinase domain. We elucidate the role of the negative regulatory region, residues 32–51, at the structural level, and present the first structures of the integral MEK1 kinase domain in ternary complexes with nucleotide and one of several allosteric inhibitors. The structures encompass both synergistic and additive allosteric inhibitors. In addition, the first structures of MEK1 in binary complexes with ADP and ATP- $\gamma$ S (but without an allosteric inhibitor) are presented. A MEK1 costructure with an ATP-competitive inhibitor, K252a, is also described for the first time. We also provide a structural basis for the differences between the synergistic and additive modes of allosteric inhibition.

Table 1: Two-Dimensional Structures of Various MEK1 Inhibitors<sup>a</sup>

K252a	U0126	Compound 1	PD325089 (the compound soaked is the (R) isomer)	PD318088
				

<sup>a</sup> Three-dimensional structural data on the protein-bound state are available for all inhibitors. PD318088 is from PDB entry 1S9J. The other four costructures with MEK1 are presented here.

The cardio-facio-cutaneous syndrome (CFC) is a rare and serious genetic disorder characterized by distinct malformations of the head, heart, and skin, mental and psychomotor retardation, and delayed growth (35). The syndrome is related to dysregulation of the MAPK pathway (36). Indeed, missense mutations in patients affected with CFC are found within BRAF, MEK1, or MEK2 kinases (36–39). The mutations lead to gain of function. The current results provide a structural rationale of how these mutations affect the kinase domain activity.

## MATERIALS AND METHODS

**Materials.** Compound **1** and PD325901 were synthesized in our laboratories. Their structures were confirmed by NMR and LC-MS. U0126 (27) and K252a were obtained from Calbiochem. ATP- $\gamma$ S and ADP were obtained from Sigma or Jena Bioscience.

**Experimental Determination of MEK1 Kinase Domain Boundaries.** The domain boundaries of the MEK1 construct used for crystallization were determined empirically by limited tryptic proteolysis. A molar ratio of 1:250 sequencing grade trypsin (Promega) to purified wild-type human np-MEK1 was used. Details of the expression, purification, and characterization of wild-type MEK1 protein have been published (40). The protease reaction was incubated at room temperature, and the reaction was stopped at 15 min intervals up to 2.5 h by the addition of PMSF and SDS sample buffer followed by immediate freezing at  $-80^{\circ}\text{C}$ . The resulting MEK1 fragments were visualized by SDS-PAGE, and the domain boundaries were analyzed by N-terminal sequencing (ABI 494 protein sequencer) and LCMS.

**Protein Expression and Purification.** The N- and C-terminal deletions and the NKF mutation (see Results) in the crystallization construct were generated by QuickChange cloning (41) using the previously described wild-type MEK1 with a TEV cleavable His<sub>6</sub> tag in the pTOPO-D vector (Invitrogen) as a template (40), Pfu polymerase (Stratagene), and several primers (see Supporting Information, Table 1).

The sequence numbering throughout this report follows the SWISSPROT database usage (entry Q02750). The gene was confirmed by sequencing and subsequently cloned into pDEST8 using the LR clonase reaction (Invitrogen). Bacu-

lovirus expressing MEK1 (37–383) NKF (N-terminal and C-terminal sequence starting and ending at positions 37 and 383, respectively, and point mutations S298N, S299K, Y300F; an additional N-terminal glycine is present at position 36 in the purified protein after TEV cleavage) was generated according to the Gateway protocol (Invitrogen).

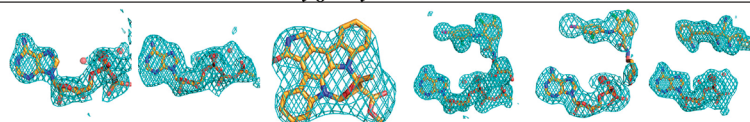
MEK1 (37–383) NKF was expressed and purified as previously described (40). The purified protein was concentrated to  $\sim 10$  mg/mL using an Amicon stirred ultrafiltration cell with a YM-10 membrane at  $4^{\circ}\text{C}$ . A 1 M magnesium acetate solution was added to the concentrated protein to give a 4-fold molar excess of Mg over protein. A 50 mM ATP- $\gamma$ S solution buffered in 20 mM HEPES, pH 7.5, 300 mM NaCl, 2 mM DTT, and 1 mM TCEP was added to the protein solution to give a 2-fold molar excess of ATP- $\gamma$ S over protein. The resulting MEK1 (37–383) NKF binary complex was incubated on ice for 10 min and filtered using a  $0.1\ \mu\text{m}$  spin filter (Amicon). The complexed protein was used immediately or stored at  $-80^{\circ}\text{C}$ .

**Crystallization Conditions.** Crystals were obtained using the hanging-drop vapor diffusion method. The MEK1 (37–383) NKF-ATP- $\gamma$ S protein-nucleotide binary complex ( $1\ \mu\text{L}$ ) in 20 mM HEPES, pH 7.5, 300 mM NaCl, 2 mM DTT, 1 mM TCEP, and 1% glycerol was mixed with  $1\ \mu\text{L}$  of distilled water and  $1\ \mu\text{L}$  of precipitant solution (0.1 M Tris-HCl, pH 8.0, 18% PEG 4000, 0.2 M calcium chloride, 3% DMSO) on the underside of a siliconized Teflon slip cover and sealed over a reservoir containing 1 mL of precipitant solution in a Qiagen EasyXtal 24-well plate. The order of addition to the coverslip was water and reservoir solution followed by protein. Crystallization plates were incubated at  $4^{\circ}\text{C}$ ; hexagonal rod crystals ( $75 \times 75 \times 250\ \mu\text{m}$ ) grew within 18–24 h. Prior to data collection, all crystals were transferred into a cryoprotective solution containing 20% PEG 4000, 0.2 M calcium chloride, 0.1 M Tris, pH 8.0, 3% DMSO, and 20% glycerol. The crystals were then flash-cooled in a nitrogen stream at 95 K or in liquid nitrogen. Crystals of the ternary MEK1-ATP- $\gamma$ S-compound **1** complex were obtained following the same protocol as for the binary complex, except for addition of the inhibitor from a 50 mM stock in 100% DMSO to a final concentration of 500  $\mu\text{M}$ .



Table 2: X-ray Data and Refinement Statistics<sup>a</sup>

Dataset	Mg <sup>2+</sup> ADP	Mg <sup>2+</sup> ATP-γS	Mg <sup>2+</sup> K-252a	Mg <sup>2+</sup> ATP-γS Compound 1	Mg <sup>2+</sup> ADP PD325089	Mg <sup>2+</sup> ADP U0126
PDB ID <sup>(1)</sup>	3EQI	3EQD	3EQF	3EQC	3EQG	3EQH
<i>Method of preparation</i>						
	Co-crystals with ATP-γS, ATP-γS hydrolysis in crystal	Co- crystallization	Soak of MEK1- ATP-γS co- crystal 1 mM 2 days	Co- crystallization	Soak of MEK1-ADP- compound 1 co-crystal at saturation 11 days	Soak of MEK1-ATP- γS co-crystal at 1 mM 6 days, ATP-γS hydrolysis in crystal
<i>X-ray diffraction data</i>						
Unit cell (P6 <sub>1</sub> 22) <sup>(2)</sup>	a=b=76.9Å c=222.6Å	a=b=77.0Å c=222.4Å	a=b=78.2Å c=223.0Å	a=b=77.2Å c=222.1Å	a=b=76.0Å c=222.3Å	a=b=76.6Å c=222.9Å
Resolution <sup>(3)</sup>	1.90Å (1.93-1.90Å)	2.10Å (2.15-2.10Å)	2.70Å (2.75-2.70Å)	1.80Å (1.83-1.80Å)	2.50Å (2.54-2.50Å)	2.00Å (2.03-2.00Å)
Complete- ness <sup>(3)</sup>	93.5% (97.6%)	97.7% (79.3%)	99.0% (99.8%)	99.5% (99.2%)	99.6% (100.0%)	99.2% (99.5%)
R <sub>sym</sub> <sup>(3)(4)</sup>	3.7% (43.6%)	6.1% (49.0%)	8.8% (47.6%)	5.6% (65.6%)	10.8% (44.1%)	7.7% (40.7%)
<I/σI> <sup>(3)(5)</sup>	24.6 (2.5)	31.1 (2.3)	12.9 (2.4)	29.4 (3.6)	19.7 (5.0)	21.4 (2.7)
<i>Refinement</i>						
R <sub>work</sub>	22.4%	21.7%	25.5%	19.9%	20.9%	22.3%
R <sub>free</sub> <sup>(6)</sup>	26.2%	24.8%	32.0%	23.5%	27.1%	25.8%
Bond lengths	0.008Å	0.008Å	0.005Å	0.017Å	0.014Å	0.008Å
angles errors <sup>(7)</sup>	1.06°	1.02°	0.81°	1.58°	1.70°	1.03°
Ramachandran distribution <sup>(8)</sup>	90.0/9.6/ 0.4/0%	92.3/7.4/ 0.4/0%	85.9/13.3/ 0.7/0%	92.5/6.8/ 0.8/0%	87.4/10.4/ 1.9/0.4%	90.0/8.5/ 1.1/0.4%
<i>Density gallery<sup>(9)</sup></i>						



<sup>a</sup> (1) Coordinates and structure factors have been deposited in the Protein Data Bank. Raw diffraction images may be obtained from T.O.F. by request. (2) The space group is P6<sub>1</sub>22 for all crystals. (3) The lower number between parentheses is for the last resolution shell. (4)  $R_{\text{sym}} = \sum |I - \langle I \rangle| / \sum I$ , where  $I$  = observed intensity and  $\langle I \rangle$  = average over Friedel and symmetry equivalents. (5) Represents an average of the intensity over by the evaluated error on intensity measurement ratio. (6)  $R_{\text{free}}$  (63) calculated using 4.9% of the total data set. The same list of free reflections is used for all refinements. (7) RMS deviations as output by the program WHAT\_CHECK (64). (8) Ratio of non-glycine non-proline residues that fall within one of the following regions of the Ramachandran plot, most favored, additional allowed, generously allowed, and disallowed, as output by the program PROCHECK (65). There are approximately 270 non-glycine non-proline residues in a structure. (9) SigmaA weighted difference omit maps calculated with the program BUSTER (44) plotted at 3.5 RMSD.

**Soaking Experiments.** For soaking ATP-competitive and non-ATP-competitive compounds, approximately three crystals were transferred into 20  $\mu$ L drops comprised of 2  $\mu$ L of compound (between 1 and 200 mM) in 100% DMSO plus 18  $\mu$ L of stabilizing solution (20% PEG 4000, 0.22 M calcium chloride, 0.11 M Tris, pH 8.0). The drop was subsequently incubated at 4 °C for 1–7 days over a reservoir containing 250  $\mu$ L of stabilizing solution in a Qiagen EasyXtal 24-well plate. The crystals were then transferred in a cryosolution and frozen as described before. The cocrystals with K252a and UO126 were obtained by soaking MEK1•ATP-γS cocrystals with 1 mM inhibitor concentration for 2–6 days. The MEK1•ADP•PD325089 costructure was obtained from a crystal of the MEK1•ADP•PD185352 ternary complex soaked with PD325089 at saturation for 11 days.

**Data Collection and Processing.** X-ray diffraction data were collected in-house using a Rigaku FR-E generator equipped with a Rigaku R-Axis 4++ image plate detector. The crystallographic data were also measured at the Advanced Photon Source (APS), sector 17, Industrial Macromolecular Crystallography Association (IMCA), ID-17 beam-

line, using an ADSC Q210 CCD detector. Data were integrated and scaled using the HKL2000 package (42).

**Structure Determination and Refinement.** The structure was solved by Molecular Replacement with the software MolRep (43), part of the CCP4 suite of programs. The starting model for molecular replacement was PDB entry 1S9J, but all subsequent structures used our first refined structure as a starting point. All refinements were performed with the programs autoBUSTER and BUSTER (44). Maps were inspected, and the model was corrected with the O graphics program (45). All ligands, cations, nucleotides, or inhibitors were added after inspection of omit sigmaA-weighted difference Fourier maps (Table 2). Dictionaries were generated using the program MakeTNT (46) from structures minimized in MacroModel and checked with the EditTNT software (46). Structure superpositions were performed using the program LSQMAN, part of the Uppsala Software Factory suite. Figures were prepared with the program PYMOL (47). Mapping of the MEK2 mutations involved in the CFC syndrome onto the MEK1 structure was performed on the basis of a sequence alignment generated with CLUSTALW (Supporting Information, Table 2).

*Evaluation of ATP- $\gamma$ S Stability in the Absence or Presence of MEK1.* A sample of apo MEK1 (37–383) NKF taken from the pool used for crystallization was diluted 5-fold using the protein buffer. Magnesium and ATP- $\gamma$ S were added in a 1:0.9 protein:nucleotide ratio, i.e., with a small excess of protein. The complex was allowed to incubate at 4 °C (the temperature at which the crystals grow). Aliquots (10  $\mu$ L) were retrieved, one immediately and others after 24, 48, and 120 h incubation. The samples were injected for ESI-LCMS analysis. Elution of ATP- $\gamma$ S and its potential hydrolyzed products (ADP, AMP, and adenosine) was achieved using weak anion-exchange liquid chromatography with a BioBasic AX column and was monitored by UV at 254 nm and electrospray ionization mass spectrometry (ESI-MS). ESI-MS was performed on a PE SCIEX API-150EX, single quadrupole mass spectrometer.

## RESULTS

*Kinase Domain Boundaries.* Attempts to crystallize full-length npMEK1 protein have been unsuccessful. As a result, we have sought to identify and crystallize the kinase domain of MEK1. Several approaches were followed to choose a crystallizable domain of MEK1. Initially, we used structural alignment with other kinases to determine the domain boundaries. The three-dimensional structures of 20 distinct kinases were examined and divided into two classes: (A) casein kinase 2 (CK2), cyclin-dependent kinase 2 (CDK2), CDK6, ERK2, c-Jun N-terminal kinase (JNK), and p38 have an insertion of  $\sim$ 35 residues in the C-terminal domain and (B) protein kinase A (PKA), calmodulin-dependent kinase, CK1, lymphocyte-specific kinase (LCK), hemopoietic cell kinase (HCK), c-Src, Abelson tyrosine kinase (Abl), p21-activated kinase (PAK), titin kinase, twitchin kinase, fibroblast growth factor receptor tyrosine kinase (FGFR TK), vascular endothelial growth factor receptor tyrosine kinase (VEGFR TK), transforming growth factor- $\beta$  receptor tyrosine kinase (TGF $\beta$ RTK), and insulin receptor kinase lack this insertion. Using Clustal W, the sequences of each of these classes align well, corresponding to the structural alignment. In order to obtain correspondence of the sequence and structural alignments for the full 20 kinases, the approximately 35 inserted residues were deleted from the six kinases in class A. MEK1 sequences from seven species and MEK2 sequences from five species were included in the sequence alignment to help to illustrate conserved elements in the family. A Clustal W multisequence alignment was performed using the 7 MEK1, the 5 MEK2, and the 20 distinct kinases of known structure. From the multisequence analysis the canonical kinase domain was deduced to be MEK1 (57–369). The construct MEK1 (57–369) was cloned and expressed in High Five cells and purified as previously described (40). While MEK1 (57–369) was highly expressed, it was also completely insoluble (data not shown).

We then determined the domain boundaries experimentally using limited proteolytic cleavage of full-length MEK1 (Figure 1). An N-terminal truncation occurs at position 36 in proteolytic cleavage experiments. No cleavage is observed near position 57, the N-terminal starting sequence suggested by homology models. Other cleavage sites, in the core kinase domain or in the proline-rich region, correspond to solvent-

exposed loops. Along with the structural data, these results indicate that residues 36–56 are an integral part of the kinase domain.

No C-terminal truncation products were detected by limited proteolysis (Figure 1). A number of considerations were used to select a C-terminus. First, a phosphorylation site, which is involved in negative feedback control of the cascade, had been previously reported at Thr 386. This suggests that the C-terminal region surrounding Thr 386 could be exposed and accessible to the appropriate kinases and possibly unstructured (19). Thr 386 is an upper limit for the C-terminus based on this interpretation. Defining the lower limit was based on other considerations. A report studying MEK1 C-terminal truncations showed that MEK1 constructs containing truncations at positions N-terminal to residue Gly 379 are found in the membrane compartments and can only be extracted with SDS (25). The authors suggest that the C-terminus contains a cellular translocation signal. On the basis of this observation, we first generated a MEK1 core kinase domain construct which incorporates a C-terminal deletion at position 369 (data not shown). The expressed protein was insoluble. This observation points to a different interpretation of the results obtained by Cha et al.: MEK1 constructs incorporating a C-terminal truncation at or before position 379 may be insoluble. The signal for cellular translocation is likely aggregated protein rather than a specific sequence. Furthermore, we note that trypsin does not digest the protein at any site located C-terminal to position 362, suggesting that residues near this position are structured and not accessible for proteolytic digest. Therefore, we assessed that the C-terminal end of the kinase domain lies at or near position 383 and selected this end point for the crystallization construct. Shortly after we obtained crystals, another crystal structure of MEK1 (62–393) was published (26). Residues 384–393 are disordered in agreement with our assessment. Residues 380–382 appear important for capping and stabilizing the packing of the C-terminal helix against the kinase core.

*Selection of a Crystallizable Construct.* The chances of obtaining crystals which diffract to high resolution are increased not only by using an appropriate protein construct but also by improving protein homogeneity. In particular, the preparation must be free of the various chemical modifications which may occur during protein expression or purification. Experiments with full-length wild-type human MEK1 show that the protein is subject to slight proteolysis (data not shown) and exogenous phosphorylation during expression (40). The site of phosphorylation and proteolysis has been identified by peptide analysis and LCMS as Ser298 (40), which is a PAK phosphorylation site (48). To eliminate both proteolysis and adventitious phosphorylation and thus optimize protein yield, the crystallization construct was mutated to S298N, S299K, or Y300F (NKF). No proteolysis or phosphorylation was observed for the MEK1 (37–383) NKF construct.

*Crystallization.* The MEK1 (37–383) NKF construct has been crystallized and the X-ray structure solved (Figure 2). The MEK1 intact kinase domain crystallizes in space group  $P6_322$  with one molecule per asymmetric unit. Both binary and ternary complexes share the same crystal packing. Crystal growth requires the presence of magnesium and a nucleotide. The best resolution is achieved with ATP- $\gamma$ S.

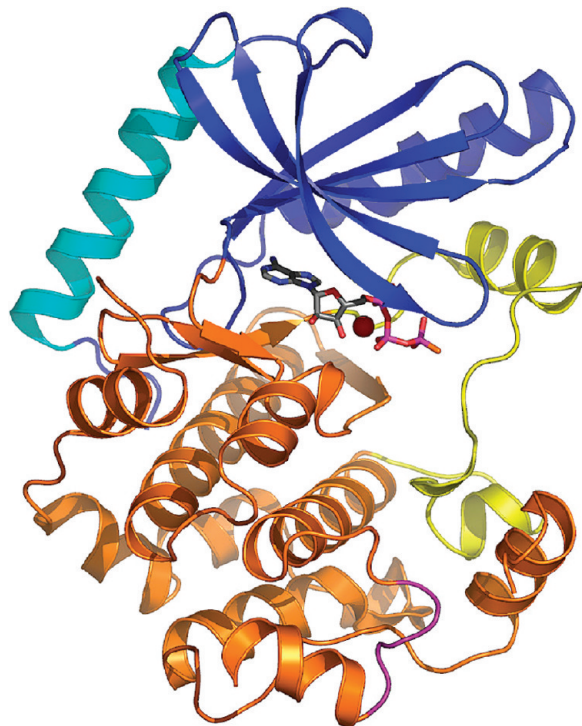


FIGURE 2: Overall view of the Mek1 kinase domain in complex with  $Mg^{2+}$  and ATP- $\gamma$ S. The protein is represented as a ribbon diagram, with the following color code: cyan, regulatory N-terminal region; yellow, T-loop; purple, proline-rich region. Other regions in the N-terminal and C-terminal lobes are colored blue and orange, respectively.  $Mg^{2+}$  is indicated as a sphere, and ATP- $\gamma$ S is shown using a ball-and-stick cartoon. The protein is oriented as for the canonical kinase domain orientation, with the N-terminal lobe at the top and the C-terminal lobe at the bottom. All figures in this paper have been prepared using PyMol (47).

Crystal growth also requires exogenous calcium, which is involved in crystal packing as discussed below. The crystallization conditions are otherwise very flexible as far as exogenous ligands are concerned. First, cocrystallization with an allosteric inhibitor is not mandatory in contrast to the MEK1 62–393 construct previously described (26). Second, crystals can be grown readily of ternary complexes with various nucleotides and allosteric inhibitors, with either synergetic or additive inhibitors such as PD325089 or U0126 (27).

**Soaking Experiments.** MEK1•ATP- $\gamma$ S cocrystals were soaked with various ATP competitive inhibitors. Examination of the OMITMAP difference Fourier density maps clearly shows total displacement of the nucleotide with the new ligand. The crystals typically diffract from 2.2 to 1.8 Å. This study presents the first X-ray crystal structure of MEK1 with an ATP-competitive inhibitor, K252a, at 2.7 Å. Structures of other binary complexes will be published elsewhere.

In contrast to the MEK1•ATP- $\gamma$ S cocrystals, ATP-competitive inhibitors fail to displace the nucleotide in soaking experiments with crystals containing an allosteric inhibitor. These observations are consistent with those obtained with the truncated kinase crystals (26). Allosteric inhibitors may be exchanged in a ternary crystal with ADP.

**Overall Comparison of the Various MEK1 (37–383) NKF Structures:** In Complex with ATP- $\gamma$ S, with or without Allosteric Inhibitors, or in Complex with ATP- $\gamma$ S Competitive Inhibitors. The six X-ray structures presented here superimpose closely for the most part. However, a helix in the

T-loop does show significant structural rearrangements (Figure 3). This helix is not well conserved among kinases. A close equivalent is CDK2 helix  $\alpha$ L12 (49), although this region is more extended in MEK1. The structures can be separated into two clusters depending on the position of this helix. The first cluster includes all of the binary complexes, with either ADP, ATP- $\gamma$ S, or K252a, and the ternary complex with the additive allosteric inhibitor U0126. The other cluster consists of all the ternary complexes with a synergistic allosteric inhibitor and either ADP or ATP- $\gamma$ S. The rearrangements in the second cluster are as follows. Helix  $\alpha$ L12 moves as a rigid body by approximately 2.0 Å relative to the first cluster. The neighboring secondary elements are also displaced but to a smaller extent. Helix C in particular moves by about 0.9 Å. The loops connecting the helices are also affected.

The polyglycine loop is the other structural element which shows significant differences among the various structures. However, these displacements are not grouped into clusters; instead, the superimposed structures form a continuum without a clear pattern. The electron density indicates disorder even when the loop is traceable. It should be noted that this loop is flexible in many kinase structures, consistent with its high glycine content. The loop is expected to be particularly flexible in MEK1 because of an additional glycine at position 79.

This study has yielded the first structure of the complete MEK1 kinase domain. Hence a comparison with the kinase core structure (PDB entry 1S9J) is particularly relevant. The MEK1 (37–383) NKF•ATP- $\gamma$ S•compound **1** ternary co-structure superposes well with that of the truncated kinase core for the most part (RMS distance of 0.9 Å). The structure of the core fragment clearly belongs to the cluster with synergetic allosteric inhibitors defined previously. However, one significant difference between the two structures is found in the T-loop. Crystal-mediated contacts play a role, and the discrepancy is likely to be a crystallization artifact: the T-loop would sterically clash with a symmetry-related molecule in the MEK1 (37–83) NKF structure if it had the same conformation as in PDB entry 1S9J. Additionally, the end of this loop is stabilized by crystal contacts in the integral kinase structure.

**Structure of the N-Terminal Helix A Regulatory Region.** Residues 39–61 are ordered (Figure 2). Residues 43–61 fold into helix A. Significant packing interactions are found all along the segment. These are mostly of a hydrophobic nature (Leu 40, Leu 42, Leu 50, and Phe 53), but polar interactions are found as well (Gln 46 to Tyr 125, Lys 59 to Phe 129 main-chain carbonyl). The region buried by the N-terminal extension involves mostly residues from the N-terminal lobe. Only residues Glu 39 and Leu 40 contact the C-terminal lobe.

**Mapping of Mutations Involved in the Cardio-Facio-Cutaneous Syndrome.** All of the MEK1/2 mutations involved in the CFC syndrome fall within the MEK1 (or MEK2) kinase domain boundaries established here. All but two mutations are found at the interface between helix A and the rest of the kinase domain (Figure 4). The exceptions are MEK1 D67N and MEK2 K273R.

**MEK1-Catalyzed Hydrolysis of ATP- $\gamma$ S.** We have collected several data sets using different MEK1 ATP- $\gamma$ S cocrystals (results not shown). The quality of the electron density maps is always excellent for the adenosine moiety



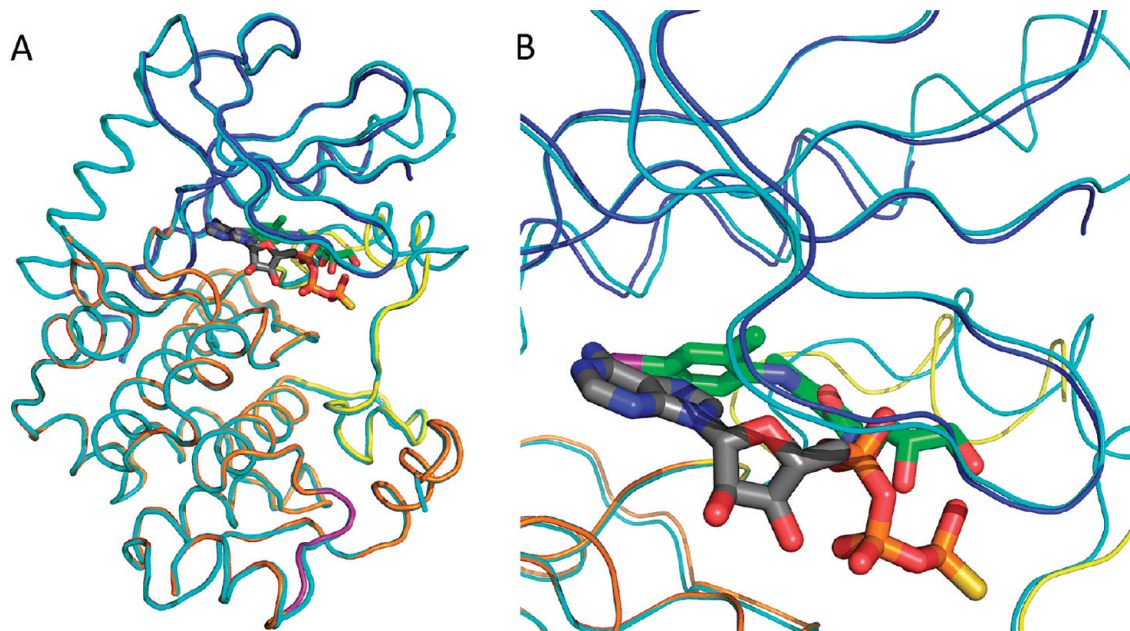


FIGURE 3: Superposition of the MEK1 kinase domain in binary complex with  $Mg^{2+}$  and ATP- $\gamma$ S and in ternary complex with  $Mg^{2+}$ , ATP- $\gamma$ S, and the allosteric inhibitor 1. Both structures are shown as a cartoon. The  $Mg^{2+}$ ATP- $\gamma$ S MEK1 binary complex is colored as in Figure 2 while the ternary complex is uniformly colored cyan. The nucleotide and the inhibitor are shown in ball-and-stick representation. The only significant structural changes are found in the T-loop (yellow). (A) Overall view in the same orientation as Figure 2. (B) Close-up to better show helix  $\alpha$ L12 (see text) and helix B motions.

and the first two phosphoryl groups. There are, however, large variations for the thiophosphoryl: the density ranges from well-defined to completely missing in the initial difference Fourier omit map. The MEK1•ADP and MEK1•ADP•U0126 structures presented here are two examples where we observe no density for the thiophosphoryl, although the crystals were grown as complexes with ATP- $\gamma$ S (Table 2). Even in the best case, a negative peak ( $-5\sigma$ ) is visible at the phosphorus atom position in the difference map after inclusion of the nucleotide in the model and refinement with an occupancy of one. These results suggest that ATP- $\gamma$ S is hydrolyzed by MEK1 in the crystal itself. MEK1-mediated ATP- $\gamma$ S hydrolysis has been reported previously without detailed characterization (50). We have therefore characterized this reaction by ESI-MS (see Supporting Information, Table 3). Surprisingly, the control (no protein) shows that ADP is present as an impurity in commercially available “pure” ATP- $\gamma$ S sources. However, no change in ADP and ATP- $\gamma$ S distribution is observed over time, indicating that ATP- $\gamma$ S is stable over at least a few days in the protein buffer. By contrast, the distribution of both nucleotides clearly changes rapidly over the course of a few days in the presence of MEK1: ATP- $\gamma$ S is completely converted to ADP after 5 days under the experimental conditions.

MEK1-mediated ATP- $\gamma$ S hydrolysis in the crystalline state has also been noticed in crystal structures of the ternary complex. Based on the electron density maps, hydrolysis seems to be as efficient with the U0126 allosteric inhibitor as without. In contrast, hydrolysis appears significantly lower in the presence of the synergic allosteric PD184352 inhibitor: the density for the thiophosphoryl is clearly present even in older crystals. Consequently, the hydrolysis rate was evaluated for the ternary complexes in solution by ESI-MS (Supporting Information, Table 3). The mass spectrometry results show good agreement with the observations from analysis of the crystallographic data: the ATP- $\gamma$ S concentra-

tion decreases with time (approximately 20% over 2 days) in presence of MEK1, or MEK1 and U0126, with a concomitant increase in ADP molarity. The results confirm our interpretation of matching ADP to the electron density map in the MEK1•ADP or MEK1•ADP•U0126 costructures presented here.

## DISCUSSION

**MEK1 Oligomerization State.** The MEK1 and MEK2 core kinase fragments have been reported to form dimers both in the crystal and in solution (26). The MEK1 and MEK2 core kinase dimer structures superimpose well (26). In particular, dimerization buries large, homologous protein surfaces. Nevertheless, the biological relevance of dimerization has been so far unclear.

The core fragment dimerization state is not reconstituted in the integral kinase domain crystal, even after taking into account the spacegroup 2-fold symmetry. Asn 78 and Val 224, which are central to the putative dimerization surface, are facing solvent and the N-terminal helical lariat from a symmetry-related molecule in the intact kinase domain, respectively. These observations are consistent with size exclusion chromatography experiments which indicate that the integral MEK1 domain is a monomer in solution (see Supporting Information, Figure 1). In addition, temperature-dependent circular dichroism measurements at different concentrations do not show changes in the midpoint temperatures of unfolding. Together, these data show that the dimerization interface found in the core structure is not biologically relevant, at least for the inactivated state of MEK1 kinase. This conclusion extends to either the ternary or binary complexes, as they basically share the same crystal packing.

The N-terminal helix A extension is not involved in the protein oligomerization state. It stacks on the opposite side

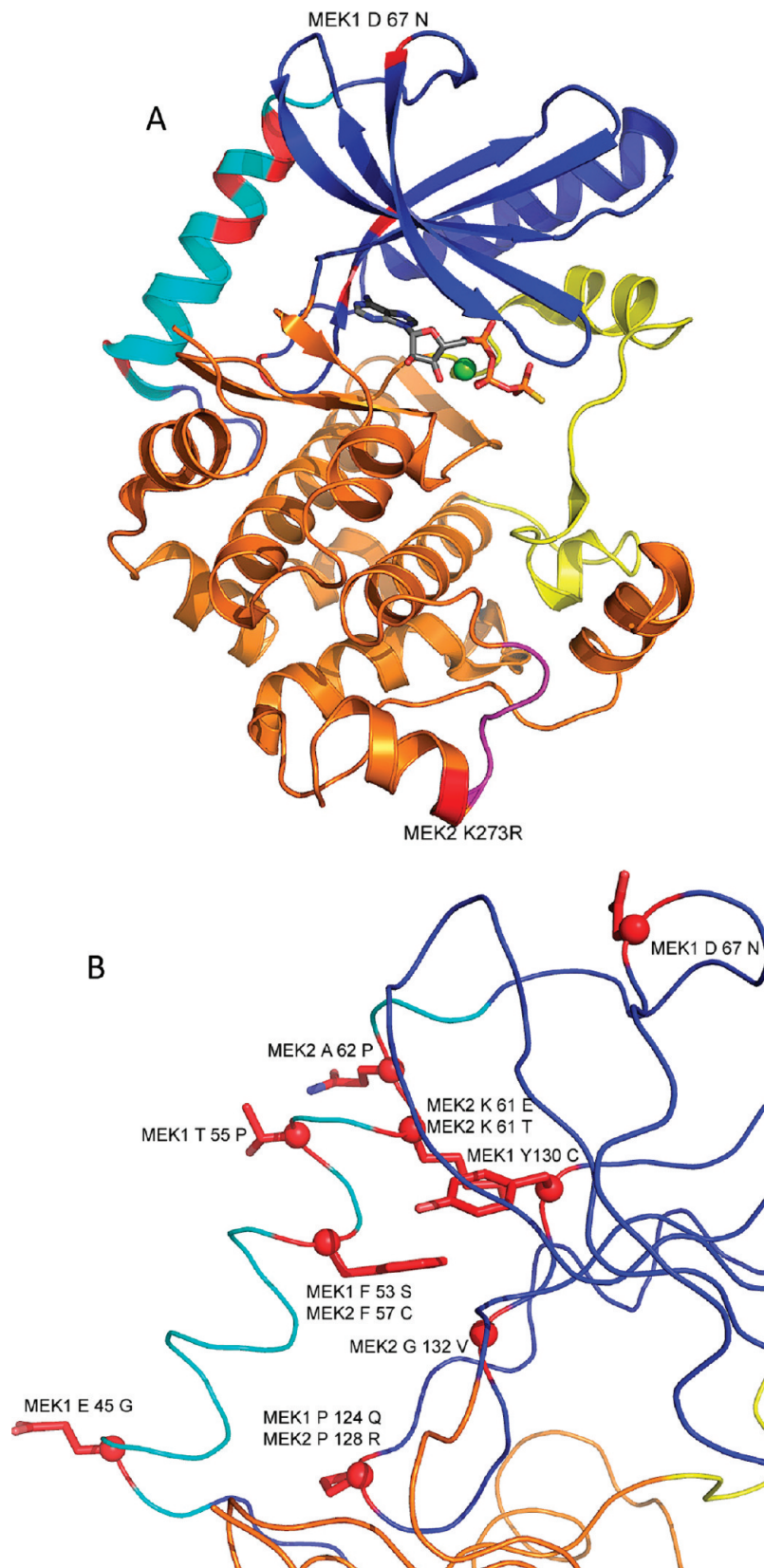


FIGURE 4: Mapping of MEK1 or MEK2 mutations involved in the CFC syndrome on the integral MEK1 kinase domain structure. (A) Overall view. The protein is represented as in Figure 2 using the same colors except that MEK1 or homologous MEK2 residues involved in the CFC syndrome are colored in green. The two mutations which are not on helix A or directly involved in its interface with the rest of the kinase domain are indicated. (B) Magnified view to show only helix A and its immediate vicinity. The orientation and the color scheme is the same as in Figure 2. The protein backbone is represented as a tube as in Figure 3. Only one mutation (MEK2 K273R) is not in view. The other mutations are indicated and their C $\alpha$  positions represented with a sphere. The side chains in the MEK1 structure are also represented (except for Gly). MEK2 mutation mapping is based on sequence alignment. All residues are conserved between MEK1 and MEK2 except for MEK2 Ala 62, which is a Gln in MEK1.



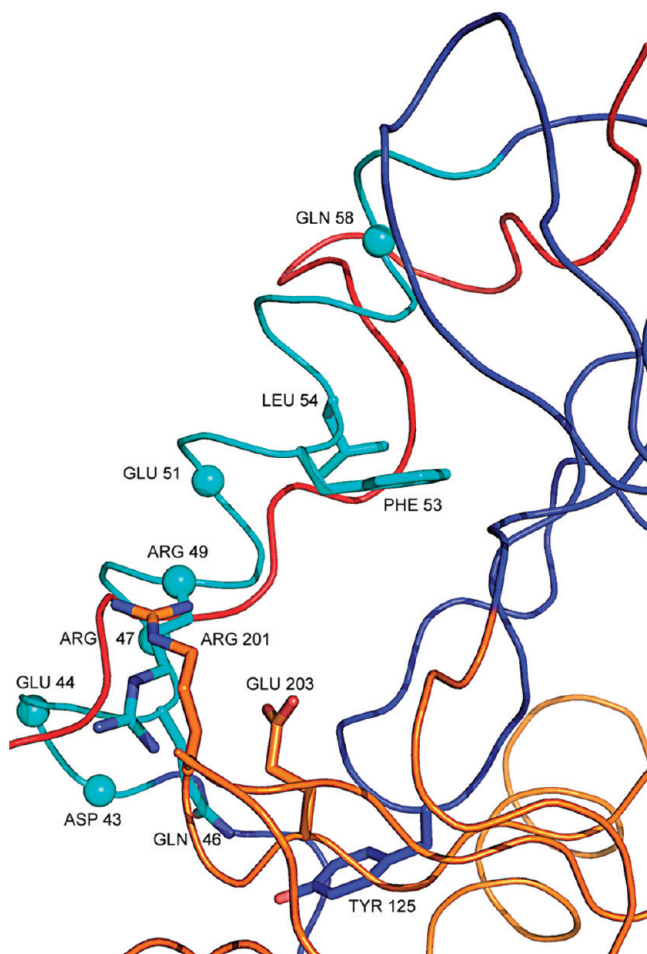


FIGURE 5: Role of helix A. The orientation and the color scheme are the same as in Figure 2 or 4. The protein backbone is represented as a tube as in Figure 3. Also represented in red is the SH2 to kinase domain linker from Abl (PDB entry 1OPK) after superposition of its kinase domain over that of MEK1. The C $\alpha$  position of several residues mentioned in Table 3 is indicated with a sphere, the amino acid name, and the amino acid number. Also shown are several side chains which are critical for the helix A–kinase core assembly.

of the protein compared to the putative dimer interface. Comparison of the truncated and integral domain structures does not point to a conformational change which would directly or indirectly prevent dimerization, such as a different elbow angle, or a cascade of structural rearrangements which propagates to the T-loop. The truncated kinase domain may be more prone to aggregation because of its lower thermal stability.

The intact kinase domain crystal structure contains a calcium cation located on a crystallographic special position. The calcium is bound in a distorted coordination geometry by two aspartates from the adjacent amino acids Asp 65 and Asp 66 and from the same residues from a neighboring protein in the crystal packing (Supporting Information, Figure 2). These residues are located in the connecting loop between helix A and strand  $\beta$ 1. The aspartates would face each other directly in the absence of the calcium ion. Crystal growth consistently occurs only in the presence of calcium in the crystallization cocktail. The surface buried in this contact is limited to the close vicinity of the calcium atom. Based on these observations, the calcium-binding site is a crystal packing artifact, and the dimer formed by application

Table 3: Summary of Truncations, Deletions, and Mutations Which Affect Helix A and MEK1 Kinase Activity<sup>a</sup>

construct	deletion	substitution	state
wild type			repressed
$\Delta$ N1	1–32		repressed
$\Delta$ N2	1–52		repressed
$\Delta$ N3	32–51		activated
Ala <sub>32–51</sub>		Ala 32–51	repressed
$\Delta$ N4	44–51		activated
Ala <sub>44–51</sub>		Ala 44–51	repressed
$\Delta$ N9	44–49		activated
Ala <sub>47–49</sub>		Ala 47–49	repressed
Pro <sub>47–49</sub>		Pro 47–49	activated
truncated domain	1–61		activated

<sup>a</sup> Taken from ref 21. For reference, the protein is ordered starting at position 38, helix A spans residues 43–59, and PDB entry 1S9J corresponds to residues 62–393 (with an initiating Met at position 61).

of the crystal 2-fold symmetry is unlikely to have biological relevance (51).

**ATP- $\gamma$ S Hydrolysis.** Hydrolysis of ATP- $\gamma$ S in the crystal has already been observed in the X-ray structures of the glycogen synthase kinase-3 $\beta$  (GSK-3 $\beta$ ) (52), focal adhesion kinase (FAK), AuroraA kinase (53), and now in MEK1. On the other hand, there are many inactivated kinases which do not hydrolyze ATP- $\gamma$ S. Surprisingly GSK-3 $\beta$ , FAK, AuroraA, and MEK1 do not share a common feature in the vicinity of the  $\gamma$ -phosphoryl which could be accountable for ATP- $\gamma$ S hydrolysis in the inactivated form. An intriguing observation comes from the fact that one allosteric inhibitor, compound 1, inhibits hydrolysis, but another allosteric inhibitor, U0126, does not. Only the former makes direct H-bond interactions with the nucleotide. These interactions may restrict hydrolysis by limiting access to the water required for the reaction. Additional studies are required to better understand MEK1-mediated ATP hydrolysis.

**Role of N-Terminal Helix A.** Overall, the MEK1 helix A is a structural feature unique to the MEK family. While N-terminal extensions have been found in a variety of other kinases, they differ from the MEK1 helix A in various ways. In some cases the extension is an extended  $\beta$ -strand. Examples are CK2, c-SRC, Abl, or LCK (54–57). Other kinases, such as cyclic adenosine monophosphate-dependent protein kinase (cAK) and p21-activated kinase 1 (PAK1), contain a helical N-terminal extension (58, 59). However, these helical lariats do not align with MEK1 helix A, except at the C-terminal end of the helix near the connection with the N-terminal lobe: most of the cAK extension runs parallel and about 14 Å away from the MEK1 helix A, and in PAK1 the axis of the N-terminal helical insertion is about 100° away from that of MEK1.

The mechanism of inhibition by helix A is best understood by comparing the MEK1 structure to that of the SH2-SH3 kinase domain assembly found in c-SRC (55), Abl (56), or HCK (60). The C-terminal end of MEK1 helix A from position 49 onward contacts the same region on the N-terminal lobe as the c-SRC, Abl, or HCK SH2 to kinase linker (Figure 5). The surface contacts between the canonical kinase lobe and the N-terminal extensions are extensive in all of these kinases. Dynamic simulations show that the SH3 and the Abl N-terminal kinase lobe form a rigid assembly (56). No similar calculations have been made for c-SRC or HCK, but the similar rigidity and function is likely based on sequence and structural homology with Abl. The kinase-

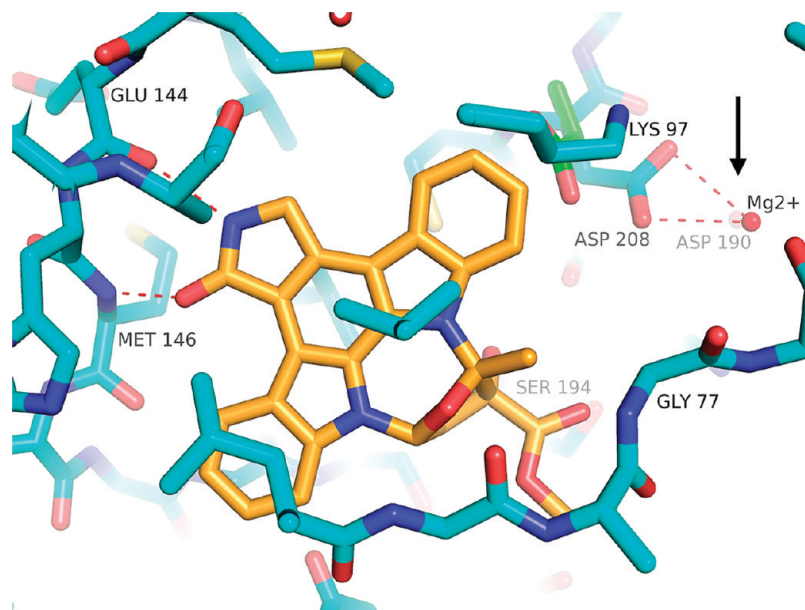


FIGURE 6: K-252a binding mode. The protein and the inhibitor are represented as sticks. Their carbon atoms are colored cyan and orange, respectively. The Asp 207 side chain as oriented in the MEK1 • ADP costructure is also shown as sticks, using green color for the carbon atoms. The magnesium cation is schematized as a red sphere. H-bond interactions are shown as red dashed lines. An arrow points to the negatively charged pocket where magnesium binds (see text).

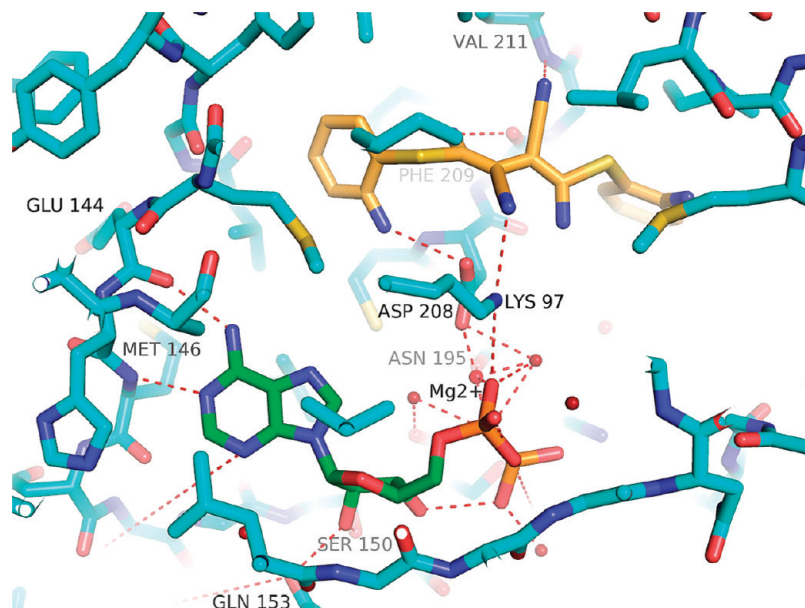


FIGURE 7: U0126 binding mode. The protein, ADP, and inhibitor are presented as sticks. Their carbon atoms are colored cyan, green, and orange, respectively. Magnesium and waters are shown as spheres. Only waters involved in the H-bond network with ADP, magnesium, or U0126 are displayed to simplify the diagram. H-bond interactions are shown as red dashed lines.

SH2 connection and the SH3 domain act as a clamp which locks the N-terminal lobe in an inactive conformation. It thus contributes to keep helix C shifted away from its active state orientation through a cascade of intramolecular contacts across the subdomain. Helix A could negatively regulate MEK1 via a similar mechanism: helix A represses enzymatic activity by stabilizing the inactive conformation with helix C shifted away from its active state orientation. However, MEK1 helix A does not involve extensive contacts with the kinase C-terminal lobe, as the SH2-SH3 domains do, and may not affect the relative orientation of the two kinase lobes (61).

The gain of function observed in several constructs made by Mansour et al. (21) (summarized in Table 3) can now be

rationalized on a structural basis by considering the amount of structural integrity left in helix A and its ability to pack against the N-terminal lobe. Enzymatic repression and constitutive activation are observed when the overall conformation of the helix is disrupted ( $\Delta N3$ ,  $\Delta N4$ ,  $\Delta N9$ , or  $\text{Pro}_{47-49}$ ; see Table 3 and Figure 5). Additionally, some deletions, such as  $\Delta N3$  and  $\Delta N9$ , further disrupt the interface between helix A and the core kinase domain by introducing an Asn or Asp, respectively, at the position previously occupied by Arg 49. This substitution leads to the loss of an H-bond between Arg 49 and Glu 203. The C-terminal half of the helix, which is the most involved in contacts with the N-terminal lobe and likely maintains helical integrity, is sufficient for repression in several variants ( $\Delta N2$ ,  $\text{Ala}_{32-51}$ ,

or Ala<sub>44–51</sub>). These constructs preserve critical interactions between the helix and the rest of the N-terminal lobe, such as the burial of Phe 53 and Leu 54, as well as H-bonds between Lys 57 and the core kinase domain. Even though the N-terminal half of helix A (43–51) is not necessary for repression, it still contributes to helical stability and binding. Specifically Asp 43 provides N-capping interactions, Gln 46 forms H-bonds with Tyr 125, and Arg 49 stacks with Arg 201 and interacts with Glu 203.

**CFC Syndrome.** The structure of the integral kinase domain helps to elucidate the role MEK1 mutations play in the disease, which was not possible on the basis of the core kinase structure alone. The mutations affect the packing of helix A in various ways. Positions Phe 53 and Lys 57 (mek2 lys 61) are central to the interface with the rest of the kinase domain (Figure 4). Other mutations in the helix are solvent-exposed, yet still affect helix A orientation: Glu45Gly may impact helix stability, while mutation of residues at position 55 or 58 (i.e., MEK2 A62P) to proline introduces a kink near the helix A C-terminus. Some mutations are not in helix A itself: it is striking that these residues contribute to the interface between the regulatory helix and the rest of the kinase domain. These include mutations in the portion of the  $\alpha 5$   $\beta$ -strand where it is closely packed against the helix at positions 128 (MEK2 G132V) and 130. It also includes a mutation at position 124 which faces the regulatory helix near residue 46.

There are two mutations outside the interface between helix A and the rest of the N-terminal lobe. Their role in MEK1 constitutive activation is unclear based on the kinase structure. They may impact docking interactions with other regulatory proteins. The first of these two mutations is Asp67Asn. It is part of the connection between helix A and the rest of the kinase domain. The other mutation is located away from the helix at position 269 (MEK2 K274R). It is the only one located in the C-terminal lobe, not far from the proline-rich region (37). Additional studies are required to understand the role of this mutation in MEK1 constitutive activation. However, the structure clearly supports the hypothesis that MEK1 inhibitors may have an application in the treatment of the disorder (36, 62).

**ATP-Competitive Inhibitor Binary Complex.** The K252a binding mode is similar to that of the related compound, staurosporine, in other kinases. The compound makes two H-bonds with the hinge region amino acids Glu 144 and Met 146 (Figure 6). The compound induces conformational changes in several locations of the binding pocket. The position of the polyglycine loop is altered and partially closes the active site cavity. This structural change adds hydrophobic interactions between the Gly 77 C $\alpha$  and a methyl substituent from the inhibitor tetrahydrofuran ring. Other structural differences are required to prevent steric clash between the inhibitor and protein. The side chains of the “gatekeeper”, Met 143, and of the catalytic residues Lys 97 and Asp 208 are rearranged to accommodate the bulky compound. A very unusual feature results from the Asp 208 side-chain rotation: its side-chain carboxylate is now facing that of Asp 190. Together, they create a negative polar pocket in which a magnesium is found (Figure 6). The cation coordination site is close to but distinct from the magnesium location in the complex with ATP- $\gamma$ S. It is also distinct from a second magnesium site found, for instance, in the FAK•ADP

complex (53). The negatively charged pocket occupied by the magnesium is readily accessible from the allosteric inhibitor binding site. It may be taken advantage of to increase the potency of this class of compounds.

**MEK1•ADP versus MEK1•ATP- $\gamma$ S.** Nonphosphorylated MEK1 binds ATP and ADP with the same, relatively high affinity, but a detailed thermodynamic analysis reveals key differences (34). The entropy change is negative upon ADP binding with a  $T\Delta S$  of  $-1.1$  kcal/mol, but it is positive with a  $T\Delta S$  of  $1.0$  kcal/mol for AMP-PNP. The enthalpy differences are  $1.9$  kcal/mol less negative for the changes upon AMP-PNP binding than they are for ADP. Overall, the differences nearly balance so that no differences in free energy and the resulting binding constants are apparent.

Comparison of the inactivated MEK1•ADP and MEK1•ATP- $\gamma$ S complex structures also reveals key structural differences which can be related to the thermodynamic data. There are two additional H-bonds in the costructure between ATP- $\gamma$ S and MEK1: one to the Lys 192 side chain and the other to the Asn 78 main-chain amine. In addition, the side chain of Asn 78 can potentially rotate and add a third hydrogen bond to ATP. This last interaction is not observed in the MEK1•ATP- $\gamma$ S costructure because the critical oxygen on the  $\gamma$ -phosphoryl is now substituted by sulfur. There are no structural differences overall between the two binary complex structures, ATP- $\gamma$ S versus ADP, except for an alteration of the polyglycine loop which is clearly induced by ATP- $\gamma$ S binding. It is this structural change which moves Asn 78 by  $1.7$  Å and allows this amino acid to H-bond with the nucleotide. The electron density also suggests that Asn 78 is more ordered in the presence of ATP- $\gamma$ S than with ADP. Ordering of the polyglycine loop seems to correlate with ordering of other residues which are next to this loop, yet not in direct contact with the nucleotide: residues Met 219 to Phe 223 clearly have better defined density in the MEK1•ATP- $\gamma$ S complex than in the MEK1•ADP costructure. Overall, the X-ray data point to significant differences in the binding mode of the two nucleotides, involving additional H-bonds and ordering of several loops for ATP- $\gamma$ S. These differences are consistent with the calorimetric data. It is important to note that the analysis presented does not take into account solvent contributions which could be thermodynamically significant.

Interestingly, ADP and ATP- $\gamma$ S bind to pMEK1 with an affinity similar to that for the nonphosphorylated kinase. However, the energetic details of the various contributions differ: entropy changes for ADP or ATP- $\gamma$ S are nearly equal and slightly positive ( $T\Delta S = 0.3$  kcal/mol and  $T\Delta S = 0.6$  kcal/mol, respectively (34)). The enthalpy differences are similar also. An interpretation consistent with these observations is that phosphorylation preorders the structure in the vicinity of the polyglycine loop. However, as mentioned before, there are many contributions to the various thermodynamic parameters that are not captured in a structural analysis. Further, the structure does not clarify why the enthalpy differences are similar for ADP and ATP- $\gamma$ S. A better understanding of the structural implications of the thermodynamic data requires the availability of the pMEK1 crystal structure.

**Binary versus Ternary Complex Structures.** PD325901 induces a conformational change in MEK1. However, these structural differences are distant from the nucleotide binding



site and unlikely to promote tighter nucleotide binding. The crystal structure of the ternary complex of MEK1•ATP•PD318088, a PD325901-like compound, shows that a network of stabilizing interactions is formed between MEK1, ATP, Mg<sup>2+</sup>, and PD318088 (26). The compound clearly mediates interactions between protein and nucleotide triphosphate, consistent with the observed synergistic stabilization and the measured predominant enthalpic contribution to  $\Delta\Delta G$  (34). The same features are observed here and are consistent with the previous study.

The mode of action of the allosteric inhibitors is still controversial. One hypothesis is that these inhibitors induce and lock the protein into an inactivated state. The comparison of the structures, in particular with U0126, indicates that the integral MEK1 kinase domain does not undergo structural changes: the protein is in the same inactive conformation as in the absence of inhibitor. The implication is that the allosteric inhibitors do not induce a new inactivated state. The inhibitor may, however, stabilize the protein in the same inactivated state as the one repressed by helix A. The fact that the whole kinase domain crystallizes with or without allosteric inhibitors, but that the domain without helix A requires an allosteric inhibitor to grow crystals, may be relevant. It suggests that the allosteric inhibitor locks the kinase domain in the same inactivated state as helix A does. A better understanding awaits the elucidation of the structure of the truncated kinase without allosteric inhibitor.

**Structural Basis for Allosteric Inhibitor with Additive ATP Contribution versus Synergistic Contribution: The Ternary Structure with U0126.** The crystal structure of the MEK1•ADP•U0126 complex shows that U0126 binds in the same pocket as PD325901. The latter interacts through several H-bonds with both ADP and ATP, although the fine details of the interactions differ between the nucleotides. By contrast, the closest distance between U0126 and ADP is about 6 Å, excluding any direct interaction between nucleotide and the inhibitor (Figure 7). We did not determine the structure of a MEK1•ATP- $\gamma$ S•U0126 complex. However, we can assume that the third phosphoryl in such a complex would be bound in the same orientation as in the ternary complex of compound 1 and ATP- $\gamma$ S. The  $\gamma$ -phosphoryl is approximately 7 Å away from U0126 in the superposition of the structures over the MEK1•ADP•U0126 model. In conclusion, the structures suggest that polar interactions between PD325901-like allosteric inhibitor and nucleotide as the main contribution for the synergistic binding observed thermodynamically.

## CONCLUSION

Kinases show great variety in the details of the activation process even though they share a common fold. Insertions or deletions in the kinase domain play a role in this diversity. This study shows that helix A is an integral part of the MEK1 kinase domain and an important regulatory element of this enzyme. The biological relevance of helix A negative regulation is clearly illustrated by the fact that mutations which may disrupt this regulation are responsible for the CFC syndrome.

MEK1 is best known as a key oncology target; however, MEK1 inhibitors may also play a role in the treatment of the CFC syndrome. While significant progress has been made toward the discovery of potent inhibitors, research has been

hampered until this study by the absence of a crystallization system which would allow for routine MEK1–ligand co-structure determination. This work should give a new impetus toward the discovery of small molecule MEK1 inhibitors.

## ACKNOWLEDGMENT

We thank Dr. Charles McNemar for performing the N-terminal sequencing, Dr. Andrew Prongay for assistance with the initial optimization of the crystals, and Dr. William Windsor for critical reading of the manuscript.

## SUPPORTING INFORMATION AVAILABLE

SEC chromatograms, a description of the primers, a picture of the calcium-binding site in the crystal, a table summarizing the N-terminal deletions discussed in this report, the MEK1/2 sequence homology, and details of the mass spectrometry data characterizing the ATP- $\gamma$ S hydrolysis. This material is available free of charge via the Internet at <http://pubs.acs.org>.

## REFERENCES

- Pages, G., Lenormand, P., L'Allemain, G., Chambard, J. C., Meloche, S., and Pouyssegur, J. (1993) Mitogen-activated protein kinases p42mapk and p44mapk are required for fibroblast proliferation. *Proc. Natl. Acad. Sci. U.S.A.* 90, 8319–8323.
- Sontag, E., Fedorov, S., Kamibayashi, C., Robbins, D., Cobb, M., and Mumby, M. (1993) The interaction of SV40 small tumor antigen with protein phosphatase 2A stimulates the map kinase pathway and induces cell proliferation. *Cell* 75, 887–897.
- Cowley, S., Paterson, H., Kemp, P., and Marshall, C. J. (1994) Activation of MAP kinase kinase is necessary and sufficient for PC12 differentiation and for transformation of NIH 3T3 cells. *Cell* 77, 841–852.
- Frost, J. A., Geppert, T. D., Cobb, M. H., and Feramisco, J. R. (1994) A requirement for extracellular signal-regulated kinase (ERK) function in the activation of AP-1 by Ha-Ras, phorbol 12-myristate 13-acetate, and serum. *Proc. Natl. Acad. Sci. U.S.A.* 91, 3844–3848.
- Mansour, S. J., Matten, W. T., Hermann, A. S., Candia, J. M., Rong, S., Fukasawa, K., Vande Woude, G. F., and Ahn, N. G. (1994) Transformation of mammalian cells by constitutively active MAP kinase kinase. *Science* 265, 966–970.
- Troppmair, J., Bruder, J. T., Munoz, H., Lloyd, P. A., Kyriakis, J., Banerjee, P., Avruch, J., and Rapp, U. R. (1994) Mitogen-activated protein kinase/extracellular signal-regulated protein kinase activation by oncogenes, serum, and 12-O-tetradecanoylphorbol-13-acetate requires Raf and is necessary for transformation. *J. Biol. Chem.* 269, 7030–7035.
- Kosako, H., Gotoh, Y., and Nishida, E. (1994) Requirement for the MAP kinase kinase/MAP kinase cascade in *Xenopus* oocyte maturation. *EMBO J.* 13, 2131–2138.
- Fukuda, M., Gotoh, Y., Tachibana, T., Dell, K., Hattori, S., Yoneda, Y., and Nishida, E. (1995) Induction of neurite outgrowth by MAP kinase in PC12 cells. *Oncogene* 11, 239–244.
- English, J. M., and Cobb, M. H. (2002) Pharmacological inhibitors of MAPK pathways. *Trends Pharmacol. Sci.* 23, 40–45.
- Pearson, G., English, J. M., White, M. A., and Cobb, M. H. (2001) ERK5 and ERK2 cooperate to regulate NF- $\kappa$ B and cell transformation. *J. Biol. Chem.* 276, 7927–7931.
- Sears, R. C., and Nevins, J. R. (2002) Signaling networks that link cell proliferation and cell fate. *J. Biol. Chem.* 277, 11617–11620.
- Lewis, T. S., Shapiro, P. S., and Ahn, N. G. (1998) Signal transduction through MAP kinase cascades. *Adv. Cancer Res.* 74, 49–139.
- Payne, D. M., Rossomando, A. J., Martino, P., Erickson, A. K., Her, J. H., Shabanowitz, J., Hunt, D. F., Weber, M. J., and Sturgill, T. W. (1991) Identification of the regulatory phosphorylation sites in pp42/mitogen-activated protein kinase (MAP kinase). *EMBO J.* 10, 885–892.
- Seger, R., Ahn, N. G., Posada, J., Munar, E. S., Jensen, A. M., Cooper, J. A., Cobb, M. H., and Krebs, E. G. (1992) Purification and characterization of mitogen-activated protein kinase activator(s)

- from epidermal growth factor-stimulated A431 cells. *J. Biol. Chem.* 267, 14373–14381.
15. Robbins, D. J., Zhen, E., Owaki, H., Vanderbilt, C. A., Ebert, D., Geppert, T. D., and Cobb, M. H. (1993) Regulation and properties of extracellular signal-regulated protein kinases 1 and 2 in vitro. *J. Biol. Chem.* 268, 5097–5105.
16. Resing, K. A., and Ahn, N. G. (1998) Deuterium exchange mass spectrometry as a probe of protein kinase activation. Analysis of wild-type and constitutively active mutants of MAP kinase kinase-1. *Biochemistry* 37, 463–475.
17. Alessi, D. R., Saito, Y., Campbell, D. G., Cohen, P., Sithanandram, G., Rapp, U., Ashworth, A., Marshall, C. J., and Cowley, S. (1994) Identification of the sites in MAP kinase kinase-1 phosphorylated by p74raf-1. *EMBO J.* 13, 1610–1619.
18. Zheng, C. F., and Guan, K. L. (1994) Activation of MEK family kinases requires phosphorylation of two conserved Ser/Thr residues. *EMBO J.* 13, 1123–1131.
19. Brunet, A., Pages, G., and Pouyssegur, J. (1994) Constitutively active mutants of MAP kinase kinase (MEK1) induce growth factor-relaxation and oncogenicity when expressed in fibroblasts. *Oncogene* 9, 3379–3387.
20. Huang, W., Kessler, D. S., and Erikson, R. L. (1995) Biochemical and biological analysis of Mek1 phosphorylation site mutants. *Mol. Biol. Cell* 6, 237–245.
21. Mansour, S. J., Candia, J. M., Matsuura, J. E., Manning, M. C., and Ahn, N. G. (1996) Interdependent domains controlling the enzymatic activity of mitogen-activated protein kinase kinase 1. *Mol. Biol. Cell* 6, 237–245.
22. Xu, B., Wilsbacher, J. L., Collisson, T., and Cobb, M. H. (1999) The N-terminal ERK-binding site of MEK1 is required for efficient feedback phosphorylation by ERK2 in vitro and ERK activation in vivo. *J. Biol. Chem.* 274, 34029–34035.
23. Fukuda, M., Gotoh, I., Gotoh, Y., and Nishida, E. (1996) Cytoplasmic localization of mitogen-activated protein kinase kinase directed by its NH<sub>2</sub>-terminal, leucine-rich short amino acid sequence, which acts as a nuclear export signal. *J. Biol. Chem.* 271, 20024–20028.
24. Fukuda, M., Gotoh, I., Adachi, M., Gotoh, Y., and Nishida, E. (1997) A novel regulatory mechanism in the mitogen-activated protein (MAP) kinase cascade. Role of nuclear export signal of MAP kinase kinase. *J. Biol. Chem.* 272, 32642–32648.
25. Cha, H., Lee, E. K., and Shapiro, P. (2001) Identification of a C-terminal region that regulates mitogen-activated protein kinase kinase-1 cytoplasmic localization and ERK activation. *J. Biol. Chem.* 276, 48494–48501.
26. Ohren, J. F., Chen, H., Pavlovsky, A., Whitehead, C., Zhang, E., Kuffa, P., Yan, C., McConnell, P., Spessard, C., Banotai, C., Mueller, W. T., Delaney, A., Omer, C., Sebolt-Leopold, J., Dudley, D. T., Leung, I. K., Flamme, C., Warmus, J., Kaufman, M., Barrett, S., Tecle, H., and Hasemann, C. A. (2004) Structures of human MAP kinase kinase 1 (MEK1) and MEK2 describe novel non-competitive kinase inhibition. *Nat. Struct. Mol. Biol.* 11, 1192–1197.
27. Favata, M. F., Horiuchi, K. Y., Manos, E. J., Daulerio, A. J., Stradley, D. A., Feeser, W. S., Van Dyk, D. E., Pitts, W. J., Earl, R. A., Hobbs, F., Copeland, R. A., Magolda, R. L., Scherle, P. A., and Trzaskos, J. M. (1998) Identification of a novel inhibitor of mitogen-activated protein kinase kinase. *J. Biol. Chem.* 273, 18623–18632.
28. Kohno, M., and Pouyssegur, J. (2006) Targeting the ERK signaling pathway in cancer therapy. *Ann. Med.* 38, 200–211.
29. Bakare, O., Ashendel, C. L., Peng, H., Zalkow, L. H., and Burgess, E. M. (2003) Synthesis and MEK1 inhibitory activities of imido-substituted 2-chloro-1,4-naphthoquinones. *Bioorg. Med. Chem.* 11, 3165–3170.
30. Delaney, A. M., Printen, J. A., Chen, H., Fauman, E. B., and Dudley, D. T. (2002) Identification of a novel mitogen-activated protein kinase kinase activation domain recognized by the inhibitor PD 184352. *Mol. Cell. Biol.* 22, 7593–7602.
31. Alessi, D. R., Cuenda, A., Cohen, P., Dudley, D. T., and Saltiel, A. R. (1995) PD 098059 is a specific inhibitor of the activation of mitogen-activated protein kinase kinase in vitro and in vivo. *J. Biol. Chem.* 270, 27489–27494.
32. Sebolt-Leopold, J. S., Dudley, D. T., Herrera, R., van Becelaere, K., Wiland, A., Gowan, R. C., Tecle, H., Barrett, S., D., Bridges, A., Przybranowski, S., Leopold, W. R., and Saltiel, A. R. (1999) Blockade of the MAP kinase pathway suppresses growth of colon tumors in vivo. *Nat. Med.* 5, 810–816.
33. Spicer, J. A., Rewcastle, G. W., Kaufman, M. D., Black, S. L., Plummer, M. S., Denny, W. A., Quin, J., Shahripour, A. B., Barrett, S., D., Whitehead, C. E., Milbank, J. B. J., Ohren, J. F., Gowan, R. C., Omer, C., Camp, H. S., Esmail, N., Moore, K., Sebolt-Leopold, J. S., Przybranowski, S., Merriman, R. L., Ortwine, D. F., Warmus, J. S., Flamme, C. M., Pavlovsky, A. G., and Tecle, H. (2007) 4-Anilino-5-carboxamido-2-pyridone derivatives as non-competitive inhibitors of mitogen-activated protein kinase kinase. *J. Med. Chem.* 50, 5090–5102.
34. Smith, C. K., and Windsor, W. T. (2007) Thermodynamics of nucleotide and non-ATP-competitive inhibitor binding to MEK1 by circular dichroism and isothermal titration calorimetry. *Biochemistry* 46, 1358–1367.
35. Reynolds, J. F., Neri, G., Hermann, J. P., Blumberg, B., Coldwell, J. G., Miles, P. V., and Opitz, J. M. (1986) New multiple congenital anomalies/mental retardation syndrome with cardio-facio-cutaneous involvement—the CFC syndrome. *Am. J. Med. Genet. A* 25, 413–427.
36. Rodriguez-Viciana, P., Tetsu, O., Tidyman, W. E., Estep, A. L., Conger, B. A., Cruz, M. S., McCormick, F., and Rauen, K. A. (2006) Germline mutations in genes within the MAPK pathway cause cardio-facio-cutaneous syndrome. *Science* 311, 1287–1290.
37. Narumi, Y., Aoki, Y., Niihori, T., Neri, G., Cave, H., Verloes, A., Nava, C., Kavamura, M. I., Okamoto, N., Kurosawa, K., Hennekam, R. C., Wilson, L. C., Gillesen-Kaesbach, G., Wiczorek, D., Lapunzina, P., Ohashi, H., Makita, Y., Kondo, I., Tsuchiya, S., Ito, E., Sameshima, K., Kato, K., Kure, S., and Matsubara, Y. (2007) Molecular and clinical characterization of cardio-facio-cutaneous (CFC) syndrome: overlapping clinical manifestations with Costello syndrome. *Am. J. Med. Genet. A* 143, 799–807.
38. Gripp, K. W., Lin, A. E., Nicholson, L., Allen, W., Cramer, A., Jones, K. L., Kutz, W., Peck, D., Rebolledo, M. A., Wheeler, P. G., Wilson, W., Al-Rahawan, M. M., Stabley, D. L., and Sol-Church, K. (2007) Further delineation of the phenotype resulting from BRAF or MEK1 germline mutations helps differentiate cardio-facio-cutaneous syndrome from Costello syndrome. *Am. J. Med. Genet. A* 143, 1472–1480.
39. Nava, C., Hanna, N., Michot, C., Pereira, S., Pouvreau, N., Niihori, T., Aoki, Y., Matsubara, Y., Arveiler, B., Lacombe, D., Pasmant, E., Parfait, B., Baumann, C., Heron, D., Sigaudy, S., Toutain, A., Rio, M., Goldenberg, A., Leheup, B., Verloes, A., and Cave, H. (2007) Cardio-facio-cutaneous and Noonan syndromes due to mutations in the RAS/MAPK signalling pathway: genotype-phenotype relationships and overlap with Costello syndrome. *J. Med. Genet.* 44, 763–771.
40. Smith, C. K., Carr, D., Mayhood, T. W., Jin, W., Gray, K., and Windsor, W. T. (2007) Expression and purification of phosphorylated and non-phosphorylated human MEK1. *Protein Expression Purif.* 52, 446–456.
41. Wang, W., and Malcolm, B. A. (1999) Two-stage PCR protocol allowing introduction of multiple mutations, deletions and insertions using QuikChange site-directed mutagenesis. *BioTechniques* 26, 680–682.
42. Otwinowski, Z., and Minor, W. (1997) Processing of X-ray diffraction data collected in oscillation mode. *Methods Enzymol.* 307–325.
43. Vagin, A., and Teplyakov, A. (1997) MOLREP: an automated program for molecular replacement. *J. Appl. Crystallogr.* 30, 1022–1025.
44. Bricogne, G. (1997) Bayesian statistical viewpoint on structure determination: Basic concepts and examples. *Methods Enzymol.* 361–423.
45. Jones, T. A. (2004) Interactive electron-density map interpretation: from INTER to O. *Acta Crystallogr., Sect. D: Biol. Crystallogr.* 60, 2115–2125.
46. Brandl, M., Smart, O. S., and Womack, T. (2008) MakeTNT 2.5.1, Global Phasing Ltd., Sheraton House, Castle Park, Cambridge CB3 0AX, U.K.
47. Delano, W. L. (2008) The PyMol Molecular Graphics System, DeLano Scientific LLC, Palo Alto, CA (<http://www.pymol.org>).
48. Frost, J. A., Steen, H., Shapiro, P., Lewis, T., Ahn, N., Shaw, P. E., and Cobb, M. H. (1997) Cross-cascade activation of ERKs and ternary complex factors by Rho family proteins. *EMBO J.* 16, 6426–6438.
49. De Bondt, H. L., Rosenblatt, J., Jancarik, J., Jones, H. D., Morgant, D. O., and Kim, S.-H. (1993) Crystal structure of cyclin-dependent kinase 2. *Nature* 363, 595–602.
50. Khokhlatchev, A. V., Canagarajah, B., Wilsbacher, J., Robinson, M., Atkinson, M., Goldsmith, E., and Cobb, M. H. (1998)

- Phosphorylation of the MAP kinase ERK2 promotes its homodimerization and nuclear translocation. *Cell* 93, 605–615.
51. Janin, J., and Rodier, F. (1995) Protein-protein interaction at crystal contacts. *Proteins* 23, 580–587.
52. Abola, E. E., Sussman, J. L., Prilusky, J., and Manning, N. O. (1997) Protein Data Bank archives of three-dimensional macromolecular structures. *Methods Enzymol.* 277, 556–571.
53. Nowakowski, J., Cronin, C. N., McRee, D. E., Knuth, M. W., Nelson, C. G., Pavletich, N. P., Rogers, J., Sang, B. C., Scheibe, D. N., Swanson, R. V., and Thompson, D. A. (2002) Structures of the cancer-related Aurora-A, FAK, and EphA2 protein kinases from nanovolume crystallography. *Structure* 10, 1659–1667.
54. Niefind, K., Putter, M., Guerra, B., Issinger, O. G., and Schomburg, D. (1999) GTP plus water mimic ATP in the active site of protein kinase CK2. *Nat. Struct. Biol.* 6, 1100–1103.
55. Xu, W., Harrison, S. C., and Eck, M. J. (1997) Three-dimensional structure of the tyrosine kinase c-Src. *Nature* 385, 595–602.
56. Nagar, B., Hantschel, O., Young, M. A., Scheffzek, K., Veach, D., Bornmann, W., Clarkson, B., Superti-Furga, G., and Kuriyan, J. (2003) Structural basis for the autoinhibition of c-Abl tyrosine kinase. *Cell* 112, 859–871.
57. Yamaguchi, H., and Hendrickson, W. A. (1996) Structural basis for activation of human lymphocyte kinase Lck upon tyrosine phosphorylation. *Nature* 384, 484–489.
58. Knighton, D. R., Zheng, J. H., Ten Eyck, L. F., Ashford, V. A., Xuong, N. H., Taylor, S. S., and Sowadski, J. M. (1991) Crystal structure of the catalytic subunit of cyclic adenosine monophosphate-dependent protein kinase. *Science* 253, 407–414.
59. Lei, M., Lu, W., Meng, W., Parrini, M. C., Eck, M. J., Mayer, B. J., and Harrison, S. C. (2000) Structure of PAK1 in an autoinhibited conformation reveals a multistage activation switch. *Cell* 102, 387–397.
60. Sicheri, F., Moarefi, I., and Kuriyan, J. (1997) Crystal structure of the Src family tyrosine kinase Hck. *Nature* 385, 602–609.
61. Breitenlechner, C. B., Kairies, N. A., Honold, K., Scheiblich, S., Koll, H., Greiter, E., Koch, S., Schafer, W., Huber, R., and Engh, R. A. (2005) Crystal structures of active SRC kinase domain complexes. *J. Mol. Biol.* 353, 222–231.
62. Senawong, T., Phuchareon, J., Ohara, O., McCormick, F., Rauen, K. A., and Tetsu, O. (2008) Germline mutations of MEK in cardio-facio-cutaneous syndrome are sensitive to MEK and RAF inhibition: implications for therapeutic options. *Hum. Mol. Genet.* 17, 419–430.
63. Brunger, A. T. (1992) Free R value: a novel statistical quantity for assessing the accuracy of crystal structures. *Nature* 355, 472–475.
64. Hoof, R. W., Vriend, G., Sander, C., and Abola, E. E. (1996) Errors in protein structures. *Nature* 381, 272.
65. Laskowski, R. A., MacArthur, M. W., Moss, D. S., and Thornton, J. M. (1993) PROCHECK: a program to check the stereochemical quality of protein structures. *J. Appl. Crystallogr.* 26, 283–291.

BI801898E